Materials Chemistry and Physics 327 (2024) 129910

Contents lists available at ScienceDirect

Materials Chemistry and Physics

journal homepage: www.elsevier.com/locate/matchemphys

# Single-domain structure of $Fe_3O_4$ nanoparticles encapsulation by magnetic surfactant $M(AOT)_2$ (M=Co, Ni)

Ebrahim Rostamabadi, Shaban Reza Ghorbani *, Hadi Arabi, Soheil Sharifi

*Department of Physics, Faculty of Science, Ferdowsi University of Mashhad, Mashhad, Iran*

## HIGHLIGHTS

- Magnetic capsules synthesized from M (AOT)2 surfactant containing Fe3O4 nanoparticles have superparamagnetic properties.
- Magnetic anisotropy interaction plays an essential role in the formation of magnetic capsule structures containing Fe3O4 nanoparticles.
- Magnetic surfactants on the capsule surface play a vital role in the interaction of anisotropy and the formation of single-domain structures.
- The distribution of nanoparticles within a capsule affects its saturation magnetic values.

## GRAPHICAL ABSTRACT

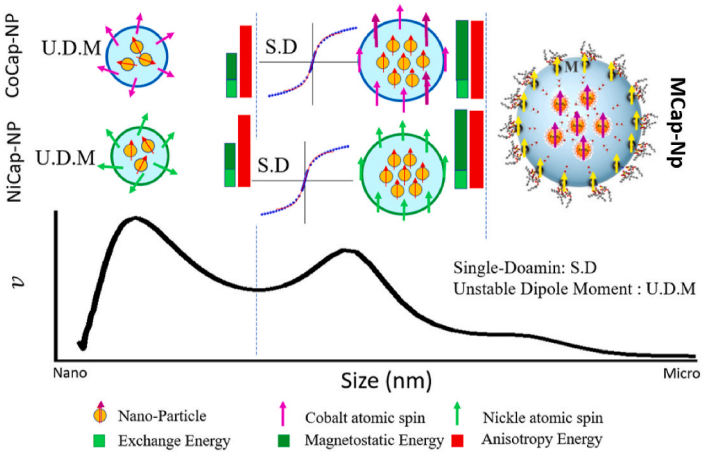


## ARTICLE INFO

*Keywords:*
Superparamagnetic
Magnetostatic
Exchange
Anisotropy
Single-domain
Saturation magnetization
Susceptibility
Coercive field

## ABSTRACT

Investigating the magnetic nanoparticle size and the effective magnetic interactions that form the magnetic domain can lead us to nanoparticles with targeted applications, such as targeted drug delivery and higher resolution MRI imaging. In this study magnetic susceptibility and coercive field properties, and the structure size range of single-domain magnetic capsules with high magnetization were obtained by structural analysis of volumetric DLS properties. In this regard, the role of exchange, anisotropy, and magnetostatic interaction was investigated in the structure of a magnetic capsule containing $Fe_3O_4$ nanoparticles (MCap-NPs). The stable capsules were synthesized in an emulsion solution with magnetic surfactants $M(AOT)_2$ (M = Co, Ni). Vibrating Sample Magnetometer (VSM) and capsule relative volume (CRV) of Dynamic Light Scattering (DLS) were used to determine the magnetic properties of the single-domain (SD) structure. The produced emulsion samples were found to have superparamagnetic properties property with saturation magnetization in the range of 2–6 $\times$ $10^{-3}$emu/g for NiCap-NPs, and 5-13 $\times$ $10^{-3}$emu/g for CoCap-NPs. The results show that nanoparticles have the most significant effect on magnetization. The coercive field, the anisotropy energy values, and the SD of $M(AOT)_2$ were determined using magnetic susceptibility distribution. The outcome results show that the surface of the magnetic capsule plays an essential role in forming a single-domain structure. It was also found that the

* Corresponding author.
*E-mail address:* sh.ghorbani@um.ac.ir (S.R. Ghorbani).

https://doi.org/10.1016/j.matchemphys.2024.129910
Received 19 May 2024; Received in revised form 21 July 2024; Accepted 27 August 2024
Available online 30 August 2024

saturation magnetization of the samples in the emulsion solution is proportional to the nanoparticle density and not to the mass of nanoparticles. All produced samples have distinct peaks in CRV versus capsule size, and each peak follows a log-normal distribution. For both samples, except for the samples with molar ratios ω of 23 (Co3 and Ni4 samples), the positions of the second and third relative volume peaks were constant at 269 ± 3 nm and 424±6 nm, respectively. The behavior of the CRV function normalized to the peak size showed a proportionality between the coercive field and the CRV.

## 1. Introduction

The main issue for the application of magnetic nanoparticle (MNPs) in biomedicine is their size, high saturation magnetism, and long-term solubility. The high saturation magnetization values of MNPs, together with their long-term solubility properties, enable easy drug delivery to cancer cells, increased image resolution in magnetic resonance imaging (MRI), and improved heat dissipation in malignant hypertension (MHT) [1]. Superparamagnetic or single-domain magnetic materials with very high saturation magnetization have very good capabilities, especially in biomedical applications. Many studies have been conducted to investigate the magnetic interactions in single-domain magnetic nanoparticles. The various collective properties such as superparamagnetism [2,3], superferromagnetism [4,5], and super-spin glass [6,7] have been observed. The superparamagnetic nanoparticles, with many applications in medicine [8–11], are an excellent example for further magnetic interactions study. The stability of colloidal solutions without aggregation of magnetic nanoparticles [12] is controlled by the balance between attractive interactions (electric dipole, van der Waals, and magnetic) and repulsive interactions (electrostatic and steric). However, the effect of magnetic interactions on general magnetic properties of the stable colloidal solutions, with targeted applications, is still under extensive investigation. The magnetic properties of these nanoparticles are based on the competition between the magnetostatic (dipole-dipole) [13–17] and exchange interactions [18–20], and the anisotropy interaction [21–23].

The micro-magnetism theory provides a correct description of static magnetization far from the ideal homogeneous approximation and the coherence limit of the Stoner-Wohlfarth model [24] for single-domain structure (SD). This theory was developed by Landau and Lifshitz [25], Brown [26], and Kittel [27]. The stationary local magnetization at any point of the sample is the result of minimizing the internal magnetic energy $E_M$ [26]:

$$E_M = E_{ex} + E_A + E_{ms} \quad (1)$$

where $E_{ex}$ is the exchange energy, $E_A$ is the anisotropy energy, and $E_{ms}$ is the magnetostatic energy [28]. According to the various change of anisotropy and magnetostatic energy, the balance of these two magnetic energies will be decisive in the stability of the magnetic structure [29]. Minimizing internal magnetic energies leads to the formation of magnetic domains without external magnetic fields [29]. The theory of micro-magnetism introduces the magnetic index of the exchange length $l_{ex}$ [30] and the hardness index $\kappa$ [31], which represents the ratio of exchange energy and anisotropy energy to magnetostatic energy, respectively. The internal magnetic energy of particle distribution with different characteristics such as size, shape, volume, anisotropy, and clustering [31] is vast. The particle properties of the wide distribution can be described by the narrow and limited distribution approximation of the Stoner-Wohlfarth model. One of the measurable characteristics of magnetization is the coercivity field, which includes the relationship between particle size and magnetic structures [32,33]

$Fe_3O_4$ magnetic nanoparticles (MIONPs), with a superparamagnetic critical size of 20 nm [34], are among the most widely used nanoparticles in various environments. An emulsion or a colloidal solution [35,36], and microfluid [37,38] of these nanoparticles have many applications. Synthesis of properly coated nanoparticles leads to better colloidal stability. The stable colloidal nanoparticles with ionic [3,39,40] and organic [41,42] coatings are used in various polar and non-polar solvents, respectively. The particle size distribution in a stable colloidal is usually relatively broad (mainly log-normal distribution [43]) and may extend from SD or superparamagnetic to multi-domain structure [44]. One of the stability methods of colloidal solutions is using the self-assembled surfactants by controlling the size and shape of particles.

Many surfactants have been studied in recent years such as the investigation of magnetic surfactant materials [45]. These types of surfactants carry magnetic atoms or molecules in their polar heads. Therefore, when they are placed in the capsule structure, they show magnetic properties. In other words, they are a particle-free ferrofluid solution. By synthesizing and performing SQID analysis, Brown et al. [46] found that AOT stable surfactant capsules have superparamagnetic properties at room temperature by adding magnetic atoms such as Ni, Fe, and Co to their polar head.

Investigating the effect of the capsule surface and nanoparticle density dispersed in the emulsion solution is useful considering the internal energy interactions. However, the effect of exchange and magnetostatic interactions in the aggregation and clusters of colloidal solution particles and their magnetic properties have been determined to some extent [47]. Nevertheless, the effect of internal magnetic interactions on single or multi-domain structure of particle aggregation is still a question.

The present work focuses on investigating the magnetic properties and volume changes of MIONP encapsulation by $M(AOT)_2$ magnetic surfactants. The novelty of encapsulating MIONPs with $M(AOT)_2$ magnetic surfactants is that it allows to control of the capsule size and volume to achieve high magnetization in superparamagnetic or magnetic single-domain materials. The magnetic structure of MIONPs in M $(AOT)_2$ spherical capsules (where M = Co, Ni) was investigated to determine the role of influential interaction. Encapsulation of MIONPs helps prevent aggregation by reducing the exposed surface area. Stable capsules containing iron oxide nanoparticles (MCap-NPs) were synthesized by changing the capsule size in the emulsion environment, using the control indices of molar ratio ω and the capsule mass fraction ratio $m_{fc}$. The effect of nanoparticles and magnetic surfactants on the magnetic properties of the capsule was investigated using VSM and volumetric DLS characterization. Structural analysis of volumetric DLS properties (as a new experimental method), magnetic susceptibility and coercive field properties, and the structure size range of single-domain magnetic capsules with high magnetization were obtained.

## 2. Experimental procedure

The Solvothermal Method was used to synthesize the MIONPs, which was reported in Ref. [48]. The results of X-ray diffraction analysis, which was showed that the MIONPs were crystallized in the cubic $Fe_3O_4$ structure with a cubic structure and average size of 4 nm [48], were previously given in Ref. [48].

Magnetic surfactant $M(AOT)_2$ (M = Co, Ni) and MIONPs with citrate ion coating were synthesized by ionic liquid method [45] and one-step solvothermal [2], respectively. FTIR characterization given in Ref. [48] was also performed to investigate new bonds. The FTIR results showed that the bond between magnetic metals (Co and Ni) and the AOT surfactant is well formed.

An emulsion solution with a magnetic capsule containing MIONPs (MCap-NPs), with a core (MIONPs) and a shell (magnetic surfactant

reverse micelle) was synthesized [48]. Two control factors, molar ratio $\omega$ and capsule mass fraction $m_{fc}$, were used to investigate the size changes of the capsules:

$$\omega = \omega_{add} + \frac{n}{2} \quad where \quad \omega_{add} = \frac{[D_2O]_{add}}{[AOT]} \tag{2}$$

where $n$ is the number of water molecules per magnetic surfactant molecule, and $\omega_{add}$ is the amount of water added to the emulsion solution. The capsule mass fraction is defined as follows:

$$m_{fc} = \frac{m_{cap}}{m_{hep} + m_{cap}} \tag{3}$$

where $m_{cap}$ and $m_{hep}$ are the capsule and n-heptane mass, respectively. For $m_{fc} = 0.2$, both NiCap-NPs and CoCap-NPs capsules were prepared with different molar ratios of $\omega = 15$, 19, 23 and 27, which were named Ni1 (Co1), Ni2 (Co2), Ni3 (Co3) and Ni4 (Co4), respectively. The samples synthesized with magnetic surfactants have nano to micrometer size distribution. Finally, the stabilized mass of the nanoparticle in the capsule was calculated by subtracting the deposited mass of the MIONPs from the initial mass.

The size and shape of the capsules were analyzed by dynamic light scattering (DLS) (VASCO™ nanoparticle size analyzer) and the magnetic properties were measured by vibrating sample magnetometer (VSM, MDK CO) with maximum field strength of 20 kO.

## 3. Experimental results

The magnetic properties of the capsules were examined using VSM measurement. The experimental data of magnetization are depicted in Fig. 1 for three states: powder, colloid solution of nanoparticles with density of 25.4 mg/cm$^3$ and 23.1 mg/cm$^3$, equivalent to a MIONPs concentration of 110 mM and 100 mM, in deionized water), and n-heptane. The results show that MIONPs in both powder state and colloidal solution have superparamagnetic behavior, while n-heptane solvent is non-magnetic.

Fig. 2 shows the magnetization as a function of magnetic field for magnetic capsules containing MIONPs (MCap-NPs with M = Ni and Co) at $m_{fc} = 0.2$, i.e., Nin and Con with n = 1–4 in n-heptane. The results show that MCap-NPs have superparamagnetic behavior. Since n-heptane solvent does not show magnetic property, the superparamagnetic behavior of the other samples is related to the MCap-NP samples. As can be seen in Fig. 2a, a change in magnetization trend was observed with increasing field for NiCap-NP samples at fields higher than 10 kOe. In comparison no trend change is observed in CoCap-NP samples. These results suggest that at a field above 10 kOe, the NiCap-NP capsules are unstable. Therefore, agglomerated $Fe_3O_4$ nanoparticles are released from the capsule separately and participate in the total magnetization, while CoCap-NP capsules remain stable, Fig. 2b.

The superparamagnetic magnetization as a function of magnetic field is usually expressed as [1]:

$$M(H) = M_s L(x) + \chi_u H \tag{4}$$

where $M_s$ is saturation magnetization, $\chi_u$ is magnetic susceptibility of unknown mass, i.e. paramagnetic and diamagnetic materials, and $L(x) = cosh\, x - 1/x$ is the Langevin function, that $x = m(H - H_C)/k_B T$, $T$ is the temperature, $k_B$ is the Boltzmann constant, $m$ is magnetic moment of the particle, and $H_C$ is the coercivity field [2]. The magnetization experimental data at room temperature were fitted by Eq. (4), shown by the solid curves in Figs. 1 and 2, and the inferred parameters are given in Table 1.

The saturation magnetization and magnetic moment of MIONPs in powder and colloid solution values are also presented in Table 1 for comparison. As can be seen in Table 1, at a magnetic field of 10 kOe, NiCap-NPs and CoCap-NPs have saturation magnetization in the range of 2–6 $\times$ $10^{-3}$emu/g and 5-13 $\times$ $10^{-3}$emu/g, respectively. In comparison the saturation magnetization of MIONPs in powder and colloidal nanoparticles in deionized water forms were approximately 10 emu/g and 0.01 emu/g (1 mg of nanoparticles per gram of colloidal solution), respectively. These results show that the saturation magnetization of the colloidal solution has changed in proportion to the mass of the nanoparticles.

The value of $H_c$ at fields $H < 100\ Oe$ for MCap-NPs samples was obtained from magnetization experimental data. The results of the coercivity field versus the mean volume size of capsules, $D_m$, are shown in Fig. 3. As can be seen in Fig. 3, the $H_c$ values of CoCap-NPs are higher than those of NiCap-NPs, but a linear behavior was observed in both Nin and Con (with n = 1–3) samples with different slopes. The sudden change in $H_c$ values of Co4 and Ni4 samples can be the direct effect of nanoparticles on the total coercive field due to the instability of the capsule and the release of nanoparticles from the capsule. The values of $H_c(Oe)$ for nanoparticles and colloidal solution of nanoparticles were about $H_c \approx 10\ Oe$, which is smaller than that of capsule's value.

The capsule relative volume (CRV = $V/V_{total}$, where $V$ is the relative volume of each capsule size and $V_{total}$ is the total volume of capsules) was extracted by DLS analysis and the results are shown in Fig. 4. In the capsule size increases in most cases, as for the Ni3 and Co1 samples, three clear peaks are observed in the CRV curve as a function of the capsule size. For NiCap-NPs as $\omega$ increases, the width of the first peak of capsule size distribution becomes narrower and the CRV increases, in contrast the second peak changes inversely except for the Ni4 sample, which has a sudden increase. However, the trend of changes in CRV of CoCap-NPs is different so that it decreases in the first peak but increases in the second peak. Furthermore, a third CRV peak appears in CoCap-NPs samples. For both NiCap-NPs and CoCap-NPs samples, the positions of the second and third peaks are constant at the capsule sizes of 269 ± 3 nm and 424±6 nm, respectively, except in the Co3 sample where the second peak is not completely formed and the Ni4 sample is bicontinuous with the formation of the emulsion phase [48].

Each peak in CRV as a function of capsule size corresponds to a stable

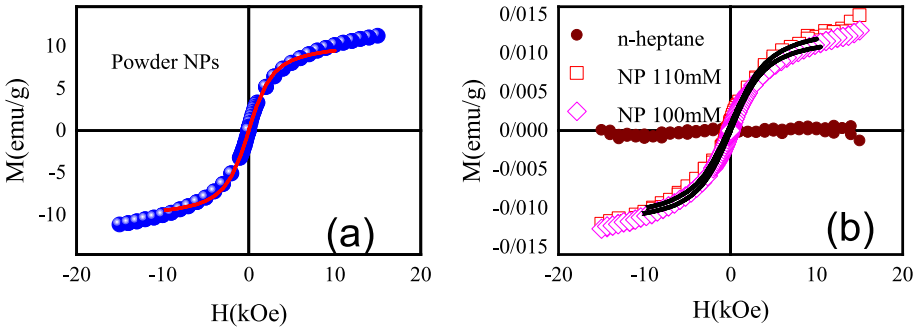


**Fig. 1.** Magnetization versus magnetic field for (a)- MIONPs in a powder form, (b)- Their colloidal solution and n-heptane. The solid curves illustrate the fitted data to Eq. (4) to the experimental data.

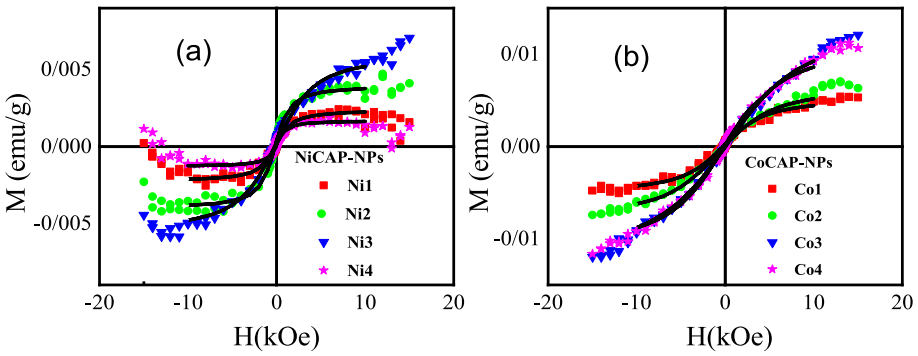


**Fig. 2.** Magnetization versus magnetic field for (a)- NiCap-NPs and (b) CoCap-NPs with different molar ratios, ω. The solid curves illustrate the fitted data to Eq. (4) to the experimental data.

**Table 1**
Saturation magnetization $M_s$ and the particle magnetic moment $m$ of MIONPs and MCap-NPs (with M = Ni and Co) at room temperature.

| | NPs | | | NiCap-NPs | | | | CoCap-NPs | | | |
|---|---|---|---|---|---|---|---|---|---|---|---|
| | powder | 110 mM | 100 mM | Ni1 | Ni2 | Ni3 | Ni4 | Co1 | Co2 | Co3 | Co4 |
| $M_s\left(\frac{emu}{g}\right)$ | 10.641 | 0.0131 | 0.0126 | 0.0023 | 0.004 | 0.006 | 0.0016 | 0.0053 | 0.0075 | 0.0133 | 0.0119 |
| $m(\mu_B)$ | 3.81 | 2.43 | 2.64 | 5.66 | 6.15 | 2.45 | 10.25 | 2.25 | 1.69 | 1.26 | 1.56 |

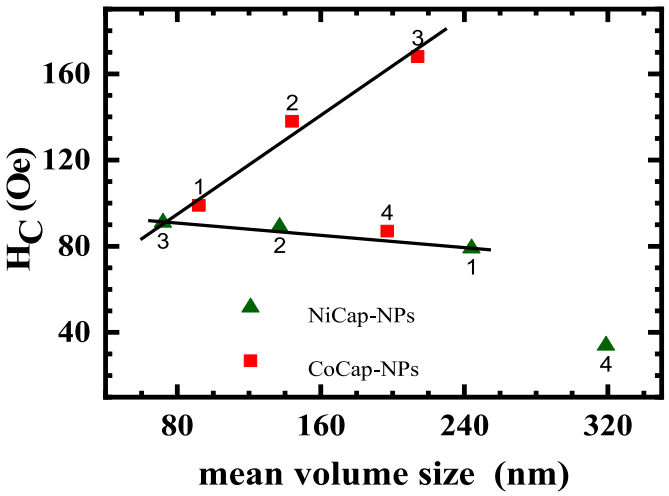


**Fig. 3.** Coercivity field versus mean volume size of the capsules, $D_m$. The numbers near each data correspond to Nin and Con samples with n = 1–4.

energy structure. To investigate the relationship between capsule size and energy stability, a log-normal distribution function was fitted to the CRV curve assuming that each peak follows the same energy and size distribution. The fitted log-normal distribution function is shown by solid curves in Fig. 4. The results of Fig. 4 show that the size distribution of nanoparticle is a log-normal distribution. The results show that the mode of the log-normal distribution function can represent the capsule size at the minimum energy of each CRV peak.

## 4. Discussion

The change of molar ratio, ω, is directly related to the average capsule size and, thus, to capsule stability. Therefore, by determining the critical limit of ω, the capsule can achieve a stable structure and establish its relationship with the maximum saturation magnetism. Fig. 5 shows the saturation magnetization values of MCap-NPs with the nanoparticle density in the emulsion solution (bottom axis). The saturation magnetization of capsules increases linearly with increasing nanoparticle density. The maximum saturation magnetization with the maximum density of MIONPs is 24.37 mg/cm$^3$ and 20.36 mg/cm$^3$ in Co3 and Ni3 samples, respectively. The results of Fig. 1 showed that the saturation magnetization in colloidal solutions depends on the mass of MIONPs. By comparing the saturation magnetization of the emulsion and colloidal solution with the same mass as MIONPs, the effective role of the magnetic capsule can be understood. Therefore, the saturation magnetization values of colloidal solution of MIONPs in deionized water were calculated with the mass of nanoparticle similar to MIONPs in emulsion samples. The results are shown in Fig. 5 (top axis). As shown in Fig. 5, the amount of saturation magnetization in the emulsion solution has a noticeable drop compared to the colloidal solution with the same mass of nanoparticles, except for sample Co4. The increase in saturation magnetization in the Co4 sample may be attributed to the formation of hollow spherical shells [47] of MIONPs inside the capsule [48]. The minimum and maximum reduction of saturation magnetization in the two emulsion and colloid states are related to Co3 and Ni3 samples, respectively.

The saturation magnetization of MCap-NPs is affected by the mass of nanoparticles, so it is expected that the change in magnetization of MCap-NPs is proportional to the nanoparticles mass. However, the saturation magnetization of MCap-NPs experiences a significant reduction compared to the colloidal solution with the same nanoparticle mass. Therefore, encapsulating nanoparticles reduces the magnetization of them. Now the question is, what is the reason for the decrease in magnetization per gram of nanoparticles in these capsules? The starting point for further discussion can be the answer to this question.

Emulsion solutions are dynamic systems in which capsules join and separate to reach thermodynamic equilibrium. This thermodynamic process leads to the formation of different size of capsules. The capsules will be stable at minimum electrical and magnetic energy. With the increase of molar ratio ω, the radial electric attraction force (the force between the surface charge of nanoparticles and the surfactant polar head) reaches its maximum value in Co3 and Ni3 samples. Nevertheless, in Co4 and Ni4 samples, the tangential electrical repulsion force (the force between the polar heads of neighbor surfactants on the capsule surface) prevents the increase of the radial force. On the other hand, the radial electric force is inversely proportional to the average capsule size and directly proportional to the nanoparticle mass density trapped in the capsule. The balance between two electrical forces leads to

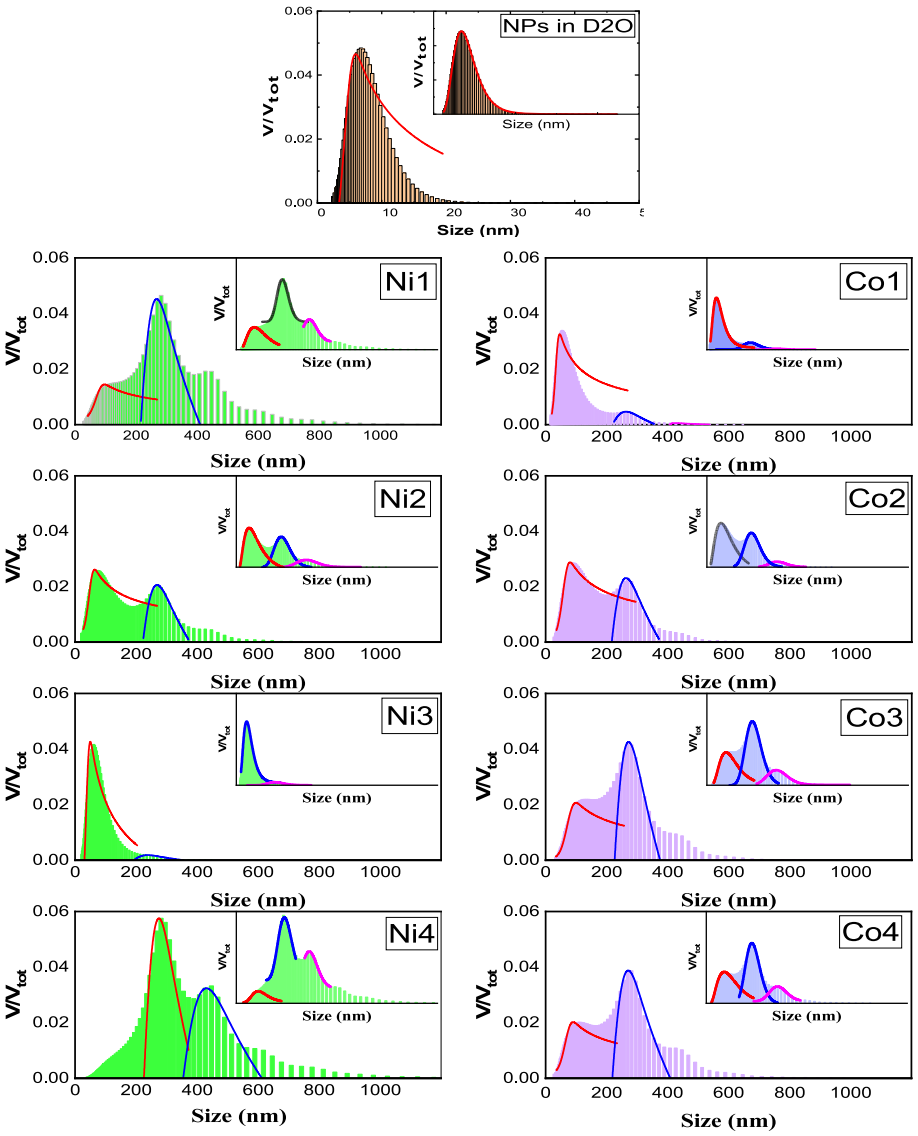


**Fig. 4.** CRV versus capsule size. top: MIONPs, left: NiCap-NPs samples, right: CoCap-NPs samples. The inset Figures and the fitted curves show the log-normal function to each peak. As can be seen in the main parts of the Figures, the fitted curves show the similarity of the CRV function and the coercive field by fitting Eq. (8) to the first and second peaks.

encapsulation, preventing precipitation, and controlling the agglomeration of nanoparticles in the emulsion solution. In addition, the magnetic properties of the capsules in the equilibrium state are influenced by the agglomeration of nanoparticles. Therefore, the balance of the magnetic structure will be by minimizing the exchange, anisotropy, and magnetostatic interactions between the spin of the surfactant counterion and the nanoparticle surface.

Although the exchange interactions between particles are effective in nanoparticles aggregation [46], the capsule is assumed to be a single particle. Vaz et al. [49] and Hergt et al. [50] deduced the indices of magnetic (such as hardness index, exchange length, and anisotropy energy) and structural properties of Co, Ni, and MIONPs. Their results show that exchange energy all three materials are roughly the same. Nevertheless, the anisotropy energy, $\boldsymbol{K_1}$, of the cobalt atom is very different from that of the other two substances. According to Brown's criteria [44] and hardness index, $\kappa$, values [49,50], Ni atom and MIONPs are soft materials, while the Co atom is a hard magnetic material.

Exchange energy and magnetostatic energy order the magnetic dipoles, while anisotropy energy opposes the order of dipoles. However, the exchange energy is low and almost the same in all samples. Therefore, the alignment of magnetic dipoles (single-domain magnetization) is achieved by increasing the magnetostatic energy compared to the anisotropy energy.

In low magnetic fields, the anisotropy energy based on Stoner-Wohlfarth model is obtained from the following relation [24]:

$$H_k = \frac{2k_{eff}}{m_s}, m_s = \frac{M_s}{v_{n-mean}} \tag{5}$$

where $k_{eff}, m_s$, and $v_{n-mean}$ $(n = 1, 2)$ are effective uniaxial magnetic anisotropy constant, volumetric saturation magnetization, and mean volume contribution of each CRV peak, respectively. The Stoner-Wohlfarth model predicted the anisotropy energy as $H_k = 0.48H_c$. Fig. 3 shows that $H_c$ has a linear behavior within the $D_m$ in the overall distribution. The positive slope of linear behavior for CoCap-NPs indicates the stability of the capsule and the increase in anisotropy energy with increasing the $D_m$. While the negative slope for NiCap-NPs is due to the instability of the capsule in larger sizes and the independent effect of MIONPs with lower $H_c$ values in the overall anisotropy energy.

Fig. 6 shows the effective uniaxial magnetic anisotropy constant $k_{eff}$, versus $D_m$ in the distribution of the total capsules for CoCap-NPs and

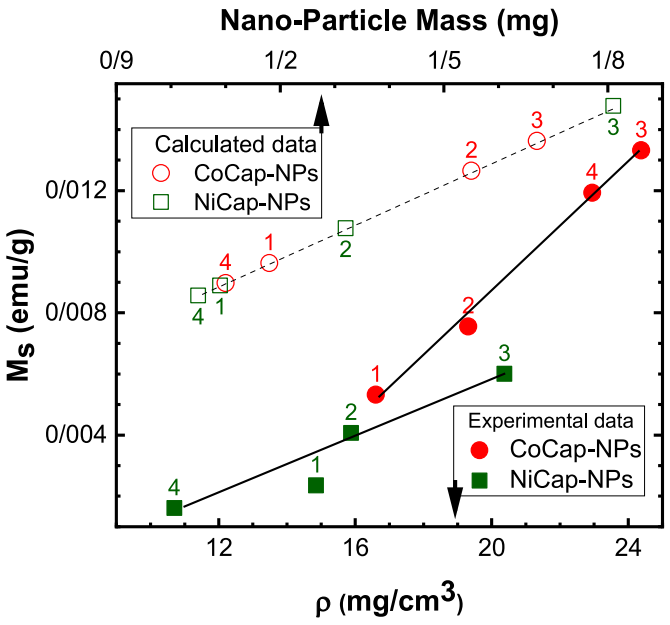


**Fig. 5.** Saturation magnetization versus MIONPs mass density in stable capsule within emulsion solution (bottom axis), and nanoparticle mass in colloidal solution (top axis). The numbers near each data correspond to Nin and Con samples with n = 1–4.

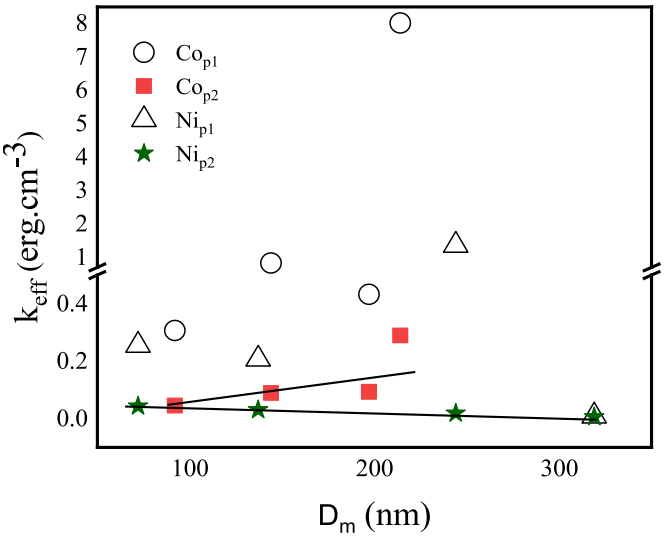


**Fig. 6.** The effective uniaxial magnetic anisotropy constant $k_{eff}$ versus the mean volume size of capsule, $D_m$, in the total distribution. Indexes p1 and p2 correspond to the CRV inside peaks of first and second.

NiCap-NPs samples. The $k_{eff}$ in the first CRV peak, unlike the $D_m$, has an uncertain behavior and higher values than the second CRV peak, in contrast to the $D_m$. While in the second CRV peak, $k_{eff}$ has a linear behavior, which indicates a SD according to the Stoner-Wohlfarth model.

In this work, an attempt will be made to discuss the role of effective interactions in the internal magnetic energy and volume distribution of the capsule using the range of changes in magnetic susceptibility and CRV. Due to the dependence of saturation magnetization on experimental skill and accurate mass measurement, saturation magnetization measurement is not a suitable method to describe the magnetic distribution of capsules. In contrast, magnetic susceptibility as a function of inherent cumulative distribution and removing the unknown mass error will have a more appropriate and complete description of the superparamagnetic behavior of the capsule distribution [51].

For all NiCap-NPs and CoCap-NPs samples, the magnetic susceptibility was calculated using the equation of $\chi = \frac{dM}{dH} - \chi_u$, where M is the saturation magnetization, and $\chi_u$ is the magnetic susceptibility of unknown mass. Fig. 7 shows the results of magnetic susceptibility versus magnetic field. As can be seen in Fig. 7, the magnetic susceptibility follows a normal distribution. The maximum magnetic susceptibility of Eq. (4) will be at $H = H_c$, and magnetic structures with different volumes also have different reactivity to the magnetic field. Therefore, the distribution with the highest response to the field can characterize the superparamagnetic behavior and the SD.

The full width at half maximum (FWHM) of the magnetic susceptibility peak is a measure of the magnetic structure distribution in capsules [52]. In Fig. 8, the right and top axes, show the FWHM of the magnetic susceptibility peak versus coercive field; And the left and bottom axes, show FWHM for the relative capsule volume $v$, versus the size of the mean capsule volume within each peak. In both samples, the behavior of FWHM in the distribution of magnetic susceptibility versus the coercive field in Nin and Con with n = 1–3 has a linear trend with a positive slope. Also, in Fig. 8, the FWHM of the first and second CRV peaks is plotted versus the size of capsule $d$ (shown in Fig. 4). Each CRV peak is a function $f_n$ of the values of the relative volume of the capsules inside each peak, which is defined as follows:

$$v_n = f_n\left(\frac{V}{V_{tot}}\right) \quad in\ the\ range\ of\ \ S_{in}\ \text{to}\ S_{fn} \tag{6}$$

where n = 1–2 is the peak number, the $S_{in}$ and $S_{fn}$ are respectively the size of the beginning and end of the log-normal distribution of each CRV peak. The results in Fig. 8 show that the change trend of the second CRV peak of the Co1(Ni1) to Co3(Ni3) samples is almost linear based on the sample order, while no such behavior is observed in the first CRV peak.

Here, the FWHM in each distribution is examined with respect to the independent distribution of each CRV peak. The changing trend of the FWHM of the magnetic susceptibility versus the coercive field and the FWHM of the second CRV peak versus $d$ are both linear in Nin and Con with n = 1–3. This shows that the capsule magnetic structure inside the second CRV peak is in the SD structure.

MIONPs with the highest magnetic susceptibility are present in both capsule samples. Therefore, the difference in magnetic susceptibility is related to the shell and size distribution of the capsules. Apart from that, the surface of the magnetic capsule plays an essential role in forming of an SD. Therefore, in the first CRV peak, the capsule surface has prevented the superparamagnetic behavior of MIONPs. In other words, they are unstable in a non-single-domain magnetic structure.

Due to the effective role of the capsule in the formation of SD and non-SD magnetic structures, some capsules do not exhibit superparamagnetic properties. Therefore, according to the superparamagnetic behavior of the samples, it can be concluded that the nanoparticles in the first CRV peak do not contribute in magnetization. We can now answer the question of the disproportion of the total saturation magnetization with the mass of the nanoparticle: the total magnetization loss due to nanoparticle encapsulation is attributed to the presence of non-single-domain capsules, which is determined by the capsule surface (magnetic surfactants).

Single domine (SD) was determined according to the results of anisotropy energy, FWHM of magnetic susceptibility, and the second peak of CRV. The second peak of CRV shows the nanoparticles distribution of different sizes with SD magnetic structure. Hergt et al. [50] obtained the relationship between the coercive field and the size of different nanoparticles in an SD as follows:

$$H_C = H_D\left(\frac{D}{D_C}\right)^{-0.6}\left[1 - \exp\left(-\frac{D}{D_C}\right)^5\right] \tag{7}$$

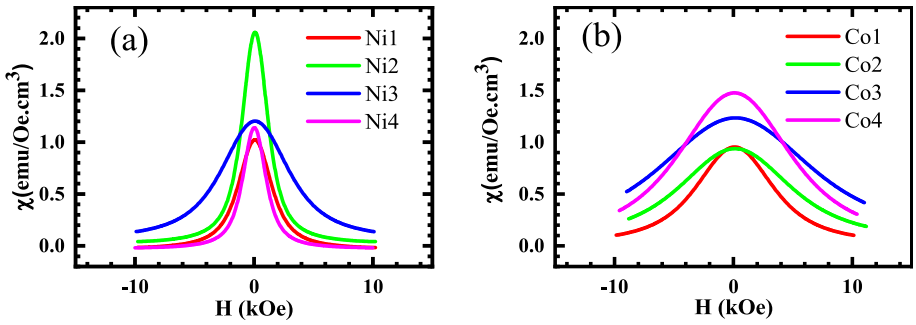


**Fig. 7.** Magnetic susceptibility versus magnetic field for a) NiCap-NPs and b) CoCap-NPs.

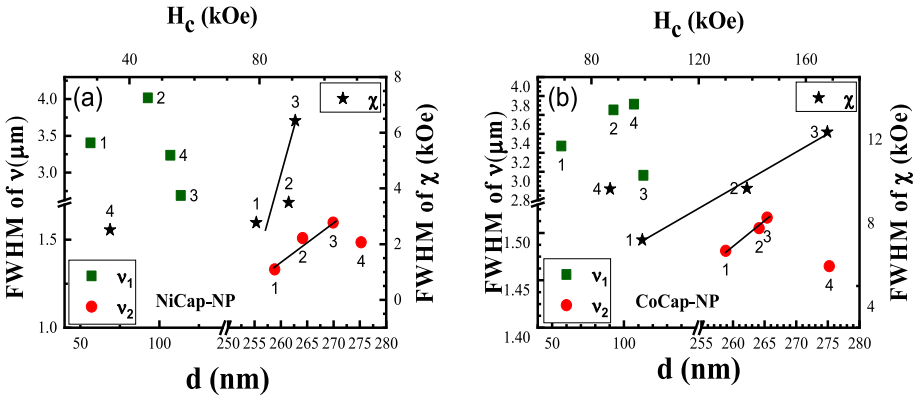


**Fig. 8.** FWHM for the relative volume of capsule $v$, versus the size of the mean capsule volume inside each peak, $d$, (left and bottom axes). Each CRV peak is calculated separately, and indices 1 and 2 correspond to the first and second CRV peaks, as shown in Fig. 4. FWHM of magnetic susceptibility peak versus coercive field (right and top axes) for a) NiCap-NPs. b) CoCap-NPs. The numbers near each data correspond to Nin and Con samples with n = 1–4.

where $D_C$ is the critical size of SD, and $H_D$ is the fitting parameter. Fig. 3 shows the variation of the coercive field versus the values of the mean volume size of the capsule, $D_m$. While $D_m$ is the mean volume size of capsule distribution. Similarly, the magnetic coercive field depends on the nanoparticle volume distribution and the SD critical size. It was also shown that the second CRV peak is related to SD capsules. Therefore, the second peak of CRV is in the form of a self-consistent distribution with different sizes of capsules, assuming that the maximum size of the second peak of CRV can be considered as the critical size of SD.

Due to the similar distribution of magnetic coercive field and CRV as a function of nanoparticle size, a similar relation as the Hergt's relation (Eq. (7)), was fitted to the first and second peaks of CRV. The following relation was used for each relative volume:

$$v_n = A_D \left(\frac{D}{D_n}\right)^{-0.6} \left[1 - \exp\left(-\frac{D}{D_n}\right)^5\right] \tag{8}$$

where $D_n$ (n = 1 and 2) is the maximum size of the $v_n$, obtained from log-normal distribution as shown in the inset of Fig. 4, and $A_D$ is the fitting parameter. Table 2 shows the results of fitting equation (8) to CRV peaks in Fig. 4 with red and blue curves for the first and second peaks, respectively. The fitting results of the similar Hergt's relationship in Fig. 4 also showed that the second CRV peak has a single-domain magnetic structure, and the first CRV peak has a non-single-domain magnetic structure. Therefore, it can be suggested that the maximum values of the second peak, $D_2$, are equivalent to the critical size of the single domain structure.

## 5. Conclusions

The results showed that the magnetic capsules synthesized from M $(AOT)_2$ surfactant containing MIONPs have superparamagnetic properties. MIONPs have the most significant effect on the saturation magnetization of capsules. The size of synthesized capsules varies from micro to nanometer. Relative volume data have distinct peaks, and each CRV peak follows a log-normal distribution. Here, the magnetic anisotropy interaction plays an essential role in forming the magnetic capsule structure containing MIONPs (MCap-NPs). The Stoner-Wohlfarth model was used to analyze the magnetic susceptibility behavior of the capsules and the anisotropy energy distribution to determine the single domain (SD) structure in the second peak of CRV. Magnetic surfactants as capsule surface plays a vital role in anisotropy interaction and SD formation. It was found that the range of the SD structure can be understood from the analysis of the FWHM parameter in the CRV distribution versus the capsule size and the magnetic susceptibility values versus the magnetic field. Part of the distribution of nanoparticles in the non-single-domain capsule causes the saturation magnetic values of the capsules to be proportional to the density of the nanoparticles, not the mass of the nanoparticles. It was shown that the experimental Hergt's relationship for coercive field values is in good agreement with the

**Table 2**
Maximum value of the first and second CRV peaks.

| | NPs in $D_2O$ | Ni1 | Ni2 | Ni3 | Ni4 | Co1 | Co2 | Co3 | Co4 |
|---|---|---|---|---|---|---|---|---|---|
| $D_1(nm)$ | 6.67 | 95.3 | 76.4 | 61.8 | 114.4 | 92.7 | 113.6 | 112.7 | 106.9 |
| $D_2(nm)$ | – | 267.8 | 273.6 | 229.8 | 265.6 | 264.1 | 269.9 | 271.8 | 271.8 |

experimental data of the second CRV peak, indicating that the second peak capsules are in the SD structure. It is suggested to use volumetric DLS analysis as a new experimental method in determining the size range of capsules in structures with high magnetization (single-domain structure) in suspension and colloidal solutions.

## CRediT authorship contribution statement

**Ebrahim Rostamabadi:** Writing – original draft, Methodology, Formal analysis, Data curation. **Shaban Reza Ghorbani:** Writing – review & editing, Writing – original draft, Supervision, Investigation, Formal analysis, Conceptualization. **Hadi Arabi:** Writing – original draft, Supervision, Investigation, Formal analysis, Conceptualization. **Soheil Sharifi:** Writing – review & editing, Supervision, Formal analysis.

## Declaration of competing interest

The authors declare that they have no known competing financial interests or personal relationships that could have appeared to influence the work reported in this paper.

## Data availability

Data will be made available on request.

## Acknowledgement

This work was supported by the Ferdowsi University of Mashhad (Grant no. 3.56784).

## References

[1] L.S. Ganapathe, M.A. Mohamed, R. Mohamad Yunus, D.D. Berhanuddin, Magnetite ($Fe_3O_4$) nanoparticles in biomedical application: from synthesis to surface functionalisation, Magnetochemistry 6 (2020) 68, https://doi.org/10.3390/magnetochemistry6040068.
[2] C.P. Bean, J.D. Livingston, Superparamagnetism, J. Appl. Phys. 30 (1959) S120–S129, https://doi.org/10.1063/1.2185850.
[3] L.H. Shen, J.F. Bao, D. Wang, Y.X. Wang, Z.W. Chen, L. Ren, X. Zhou, X. Bin Ke, M. Chen, A.Q. Yang, One-step synthesis of monodisperse, water-soluble ultra-small Fe3O4 nanoparticles for potential bio-application, Nanoscale 5 (2013) 2133–2141, https://doi.org/10.1039/c2nr33840h.
[4] S. Tong, H. Zhu, G. Bao, Magnetic iron oxide nanoparticles for disease detection and therapy, Mater. Today 31 (2019) 86–99, https://doi.org/10.1016/j.mattod.2019.06.003.
[5] K. Witte, W. Bodnar, T. Mix, N. Schell, G. Fulda, T.G. Woodcock, E. Burkel, A detailed study on the transition from the blocked to the superparamagnetic state of reduction-precipitated iron oxide nanoparticles, J. Magn. Magn Mater. 403 (2016) 103–113, https://doi.org/10.1016/j.jmmm.2015.11.074.
[6] M.S. Andersson, Nanoparticle magnetism: superspin glasses, J. Nanosci. Nanotechnol. 19 (2019) 4903–4910, https://doi.org/10.1166/jnn.2019.16798.
[7] J.A. De Toro, S.S. Lee, R. Mathieu, P.S. Normile, D. Salazar, J.L. Cheong, P. Muñiz, J.M. Riveiro, M. Hillenkamp, A. Tamion, F. Tournus, P. Nordblad, Ideal superspin glass behaviour in a random-close-packed ensemble of maghemite nanoparticles, J. Phys. Conf. 521 (2014) 012011, https://doi.org/10.1088/1742-6596/521/1/012011.
[8] I. Obaidat, B. Issa, Y. Haik, Magnetic properties of magnetic nanoparticles for efficient hyperthermia, Nanomaterials 5 (2015) 63–89, https://doi.org/10.3390/nano5010063.
[9] B. Thiesen, A. Jordan, Clinical applications of magnetic nanoparticles for hyperthermia, Int. J. Hyperther. 24 (2008) 467–474, https://doi.org/10.1080/02656730802104757.
[10] V.K. Chugh, S. Liang, D. Tonini, R. Saha, J. Liu, P. Yari, V.D. Krishna, M.C.-J. Cheeran, K. Wu, J.-P. Wang, Static and dynamic magnetization responses of self-assembled magnetic nanoparticle chains, J. Phys. Chem. C (2023), https://doi.org/10.1021/acs.jpcc.3c03755.
[11] C.L. Dennis, R. Ivkov, Physics of heat generation using magnetic nanoparticles for hyperthermia, Int. J. Hyperther. 29 (2013) 715–729, https://doi.org/10.3109/02656736.2013.836758.
[12] C. Pfeiffer, C. Rehbock, D. Hühn, C. Carrillo-Carrion, D.J. de Aberasturi, V. Merk, S. Barcikowski, W.J. Parak, Interaction of colloidal nanoparticles with their local environment: the (ionic) nanoenvironment around nanoparticles is different from bulk and determines the physico-chemical properties of the nanoparticles, J. R. Soc. Interface 11 (2014) 20130931, https://doi.org/10.1098/rsif.2013.0931.
[13] A.V. Ambarov, V.S. Zverev, E.A. Elfimova, Dynamic response of interacting superparamagnetic particles with aligned easy magnetization axes, J. Magn. Magn Mater. 497 (2020) 166010, https://doi.org/10.1016/j.jmmm.2019.166010.
[14] P. Allia, M. Coisson, P. Tiberto, F. Vinai, M. Knobel, M. Novak, W. Nunes, Granular Cu-Co alloys as interacting superparamagnets, Phys. Rev. B 64 (2001) 144420, https://doi.org/10.1103/PhysRevB.64.144420.
[15] R. Fu, Y. Yan, C. Roberts, Z. Liu, Y. Chen, The role of dipole interactions in hyperthermia heating colloidal clusters of densely-packed superparamagnetic nanoparticles, Sci. Rep. 8 (2018) 4704, https://doi.org/10.1038/s41598-018-23225-5.
[16] P.-M. Déjardin, Magnetic relaxation of a system of superparamagnetic particles weakly coupled by dipole-dipole interactions, J. Appl. Phys. 110 (2011), https://doi.org/10.1063/1.3665886.
[17] G.Y. Vélez, A. Encinas, Superparamagnetic relaxation in interacting magnetic particle assemblies, J. Supercond. Nov. Magnetism 32 (2019) 2259–2265, https://doi.org/10.1007/s10948-018-4956-5.
[18] H. Kachkachi, Effect of exchange interaction on superparamagnetic relaxation, Europhys. Lett. 62 (2003) 650–656, https://doi.org/10.1209/epl/i2003-00423-y.
[19] S. Mørup, E. Tronc, Superparamagnetic relaxation of weakly interacting particles, Phys. Rev. Lett. 72 (1994) 3278–3281, https://doi.org/10.1103/PhysRevLett.72.3278.
[20] J.C.R. de Araújo, C.A. de Moraes Iglesias, R.B. da Silva, S. Araujo Barbosa, J. Xavier, E.D. da Silva Filho, J.L. Cardozo Fonseca, P.B. Souza, C. Campos Plá Cid, F.L. de A. Machado, E.F. da Silva, M. Gamino, S.N. de Medeiros, M.A. Correa, F. Bohn, Experimental evidence of exchange forces between nanoparticles in a superparamagnetic system, J. Phys. Appl. Phys. 55 (2022) 365002, https://doi.org/10.1088/1361-6463/ac7268.
[21] S.M. Fotukian, A. Barati, M. Soleymani, A.M. Alizadeh, Solvothermal synthesis of CuFe2O4 and Fe3O4 nanoparticles with high heating efficiency for magnetic hyperthermia application, J. Alloys Compd. 816 (2020) 152548, https://doi.org/10.1016/j.jallcom.2019.152548.
[22] S.Y. An, Characterization of mössbauer and superparamagnetic properties in maghemite nanoparticles synthesized by a sol–gel method, J. Electron. Mater. 52 (2023) 6308–6315, https://doi.org/10.1007/s11664-023-10569-6.
[23] Y. Prado, N. Daffé, A. Michel, T. Georgelin, N. Yaacoub, J.-M. Grenèche, F. Choueikani, E. Otero, P. Ohresser, M.-A. Arrio, C. Cartier-dit-Moulin, P. Sainctavit, B. Fleury, V. Dupuis, L. Lisnard, J. Fresnais, Enhancing the magnetic anisotropy of maghemite nanoparticles via the surface coordination of molecular complexes, Nat. Commun. 6 (2015) 10139, https://doi.org/10.1038/ncomms10139.
[24] P.T.E.C. Stoner, E.P. Wohlfarth, A mechanism of magnetic hysteresis in heterogeneous alloys, Phil. Trans. Roy. Soc. Lond. Math. Phys. Sci. 240 (1948) 599–642, https://doi.org/10.1098/rsta.1948.0007.
[25] L. Landau, E. Lifshitz, On the theory of the dispersion of magnetic permeability in ferromagnetic bodies, in: Perspectives in Theoretical Physics, Elsevier, 1992, pp. 51–65, https://doi.org/10.1016/B978-0-08-036364-6.50008-9.
[26] W.F. Brown, The effect of dislocations on magnetization near saturation, Phys. Rev. 60 (1941) 139–147, https://doi.org/10.1103/PhysRev.60.139.
[27] C. Kittel, Physical theory of ferromagnetic domains, Rev. Mod. Phys. 21 (1949) 541–583, https://doi.org/10.1103/RevModPhys.21.541.
[28] A.P. Guimaraes, Magnetism and Magnetic Resonance in Solidso Title, first ed., Wiley-VCH, New York, 1998.
[29] C. Kittel, J.K. Galt, in: Ferromagnetic Domain Theory, 1956, pp. 437–564, https://doi.org/10.1016/S0081-1947(08)60136-8.
[30] G.S. Abo, Y.-K. Hong, J. Park, J. Lee, W. Lee, B.-C. Choi, Definition of magnetic exchange length, IEEE Trans. Magn. 49 (2013) 4937–4939, https://doi.org/10.1109/TMAG.2013.2258028.
[31] A.P. Guimarães, in: The Basis of Nanomagnetism, 2009, pp. 1–20, https://doi.org/10.1007/978-3-642-01482-6_1.
[32] E.F. Kneller, F.E. Luborsky, Particle size dependence of coercivity and remanence of single-domain particles, J. Appl. Phys. 34 (1963) 656–658, https://doi.org/10.1063/1.1729324.
[33] J.D. Livingston, A review of coercivity mechanisms (invited), J. Appl. Phys. 52 (1981) 2544–2548, https://doi.org/10.1063/1.328996.
[34] Q. Li, C.W. Kartikowati, S. Horie, T. Ogi, T. Iwaki, K. Okuyama, Correlation between particle size/domain structure and magnetic properties of highly crystalline Fe3O4 nanoparticles, Sci. Rep. 7 (2017) 9894, https://doi.org/10.1038/s41598-017-09897-5.
[35] J. Philip, J.M. Laskar, B. Raj, Magnetic field induced extinction of light in a suspension of Fe3O4 nanoparticles, Appl. Phys. Lett. 92 (2008), https://doi.org/10.1063/1.2939100.
[36] A. Zhu, L. Yuan, T. Liao, Suspension of Fe3O4 nanoparticles stabilized by chitosan and o-carboxymethylchitosan, Int. J. Pharm. 350 (2008) 361–368, https://doi.org/10.1016/j.ijpharm.2007.09.004.
[37] J. Choi, S. Han, H. Kim, E.-H. Sohn, H.J. Choi, Y. Seo, Suspensions of hollow polydivinylbenzene nanoparticles decorated with Fe3O4 nanoparticles as magnetorheological fluids for microfluidics applications, ACS Appl. Nano Mater. 2 (2019) 6939–6947, https://doi.org/10.1021/acsanm.9b01420.
[38] F. Figueredo, P.T. Garcia, E. Cortón, W.K.T. Coltro, Enhanced analytical performance of paper microfluidic devices by using Fe3O4 nanoparticles, MWCNT, and graphene oxide, ACS Appl. Mater. Interfaces 8 (2016) 11–15, https://doi.org/10.1021/acsami.5b10027.
[39] J.-D. Hu, Y. Zevi, X.-M. Kou, J. Xiao, X.-J. Wang, Y. Jin, Effect of dissolved organic matter on the stability of magnetite nanoparticles under different pH and ionic strength conditions, Sci. Total Environ. 408 (2010) 3477–3489, https://doi.org/10.1016/j.scitotenv.2010.03.033.

[40] Y. Lin, J. Li, L. Lin, X. Liu, L. Chen, D. Li, The structure of modified Fe-Ni bioxide composite nanoparticles using Fe(NO3)3, Advances in Nanoparticles. 02 (2013) 294–300, https://doi.org/10.4236/anp.2013.24040.
[41] M. Baalousha, A. Manciulea, S. Cumberland, K. Kendall, J.R. Lead, Aggregation and surface properties of iron oxide nanoparticles: influence of pH and natural organic matter, Environ. Toxicol. Chem. 27 (2008) 1875, https://doi.org/10.1897/07-559.1.
[42] M. Baalousha, Aggregation and disaggregation of iron oxide nanoparticles: influence of particle concentration, pH and natural organic matter, Sci. Total Environ. 407 (2009) 2093–2101, https://doi.org/10.1016/j.scitotenv.2008.11.022.
[43] K. O'Grady, A. Bradbury, in: Particle Size Analysis in Ferrofluids, Journal of Magnetism and Magnetic Materials, 1983, pp. 91–94, https://doi.org/10.1016/0304-8853(83)90407-9 [1] K. O'Grady, A. Bradbury, Particle Size Analysis in Ferrofluids, Journal of Magnetism and Magnetic Materials. 39 (1983) 91–94. Https://Doi.Org/10.1016/0304-8853(83)90407-9. 39.
[44] W.F. Brown, The fundamental theorem of fine-ferromagnetic-particle theory, J. Appl. Phys. 39 (1968) 993–994, https://doi.org/10.1063/1.1656363.
[45] F. Shehzad, S.M.S. Hussain, A.A. Adewunmi, A. Mahboob, M. Murtaza, M.S. Kamal, Magnetic surfactants: a review of recent progress in synthesis and applications, Adv. Colloid Interface Sci. 293 (2021) 102441, https://doi.org/10.1016/j.cis.2021.102441.
[46] P. Brown, C.P. Butts, J. Eastoe, S. Glatzel, I. Grillo, S.H. Hall, S. Rogers, K. Trickett, Microemulsions as tunable nanomagnets, Soft Matter 8 (2012) 11609–11612, https://doi.org/10.1039/c2sm26827b.
[47] L. Gutiérrez, L. de la Cueva, M. Moros, E. Mazarío, S. de Bernardo, J.M. de la Fuente, M.P. Morales, G. Salas, Aggregation effects on the magnetic properties of iron oxide colloids, Nanotechnology 30 (2019) 112001, https://doi.org/10.1088/1361-6528/aafbff.
[48] E. Rostamabadi, S.R. Ghorbani, H. Arabi, S. Sharifi, Effect of the electrical charge interactions on encapsulation of Fe3O4 nanoparticle by magnetic surfactant M (AOT)2 (M = Co, Ni and Mn), J. Mol. Liq. (2024) 124233, https://doi.org/10.1016/j.molliq.2024.124233.
[49] C.A.F. Vaz, J.A.C. Bland, G. Lauhoff, Magnetism in ultrathin film structures, Rep. Prog. Phys. 71 (2008), https://doi.org/10.1088/0034-4885/71/5/056501.
[50] R. Hergt, S. Dutz, M. Röder, Effects of size distribution on hysteresis losses of magnetic nanoparticles for hyperthermia, J. Phys. Condens. Matter 20 (2008), https://doi.org/10.1088/0953-8984/20/38/385214.
[51] K.M. Kirkpatrick, B.H. Zhou, P.C. Bunting, J.D. Rinehart, Quantifying superparamagnetic signatures in nanoparticle magnetite: a generalized approach for physically meaningful statistics and synthesis diagnostics, Chem. Sci. 14 (2023) 7589–7594, https://doi.org/10.1039/d3sc02113k.
[52] K. Riahi, M.M. van de Loosdrecht, L. Alic, B. ten Haken, Assessment of differential magnetic susceptibility in nanoparticles: effects of changes in viscosity and immobilisation, J. Magn. Magn Mater. (2020) 514, https://doi.org/10.1016/j.jmmm.2020.167238, 167238.